HOKKAIDO UNIVERSITY

Title	Detailed Investigation of the Structural, Thermal, and Electronic Properties of Gold Isocyanide Complexes with Mechano-Triggered Single-Crystal-to-Single-Crystal Phase Transitions
Author(s)	Seki, Tomohiro; Sakurada, Kenta; Muromoto, Mai et al.
Citation	Chemistry-A European journal, 22(6), 1968-1978 https://doi.org/10.1002/chem.201503721
Issue Date	2016-02-06
Doc URL	https://hdl.handle.net/2115/64466
Rights	"This is the peer reviewed version of the following article: Chemistry A European journal, 22(6) February 2016 Pages 1968-1978, which has been published in final form at [Link to final article using the 10.1002/chem.201503721. This article may be used for non-commercial purposes in accordance With Wiley-VCH Terms and Conditions for self-archiving".
Type	journal article
File Information	Seki-Chemistry22(6).pdf

Hokkaido University Collection of Scholarly and Academic Papers : HUSCAP

Detailed Investigation of the Structural, Thermal, and Electronic Properties of Gold Isocyanide Complexes with Mechano-Triggered Single Crystal to Single Crystal Phase Transitions

Tomohiro Seki,[a] Kenta Sakurada,[a] Mai Muromoto,[a] Shu Seki[b,c] and Hajime Ito*[a]

Abstract: Mechano-induced phase transitions in organic crystalline materials that alter their properties have received much attention. However, most mechano-responsive molecular crystals exhibit crystal to amorphous phase transitions on mechanical stimulation, and the intermolecular interaction patterns in the daughter phase are difficult to characterize. We investigated phenyl(phenylisocyanide)gold(I) (**1**) and phenyl(3,5-dimethylphenylisocyanide)gold(I) (**2**) complexes that exhibit a mechano-triggered single crystal to single crystal phase transition. Previous reports of **1** and **2** focused on relationships between the crystalline structures and photoluminescence properties; in this work we have focused on other aspects. The face index measurements of **1** and **2** before and after the mechano-induced phase transitions indicate they undergo non-epitaxial phase transitions without a rigorous orientational relationship between the mother and daughter phases. Differential scanning calorimetry analyses revealed the phase transition of **1** to be enthalpically driven by the formation of new aurophilic interactions. In contrast, the phase transition of **2** is entropically driven, with an empty void in the mother phase, not present in the daughter phase. Scanning electron microscopy observation showed that the degree of the charging effect of both **1** and **2** was changed by the phase transitions, suggesting that the formation of the aurophilic interactions affords more effective conductive pathways. Moreover, flash-photolysis time resolved microwave conductivity measurements revealed that **1** increased in conductivity after the phase change, whereas the conductivity of **2** decreased. These contrasting results were explained by the different patterns in the aurophilic interactions. Finally, an intriguing *disappearing polymorphism* of **2** is reported, in which a polymorph form could not be obtained again after some period of time even with repeated trials. The present studies provide us with a variety of hitherto unknown insights into mechano-responsive molecular crystals, which help us understand the phase transition behaviors upon mechanical stimulation and establish rational design principles.

Introduction

Phase transitions of organic crystalline materials have received considerable attention.[1–5] A molecule capable of forming different crystalline structures generally shows phase-dependent distinct properties, such as solubility, melting temperature, size, elasticity, color, and photoluminescence, and these properties can be switched upon a phase transition. Various types of external stimulation, such as heating/cooling,[6,7] photoirradiation,[8] solvent vapor,[9–13] and the application of mechanical stimulation,[14–18] can induce the phase transitions in molecular crystals followed by the changes in various properties of the material.

Single crystal to single crystal (SCSC) phase transitions are one particular type of phase transitions seen in crystalline materials. SCSC phase transitions are generally scarce because the high quality ordering of molecules in the crystal and the macroscopic integrity has to be retained through the phase transition. Owing to recent developments in single crystal X-ray diffraction instruments, an increasing number of the SCSC phase transitions have been reported.[6–8,13,19–31] This special phase transition phenomenon is highly attractive because the detailed molecular arrangements before and after the phase transition can be fully elucidated by single crystal X-ray crystallography. Based on such detailed microscopic structural information, we can determine the origin of the macroscopic property changes. For example, Irie's group illustrated that photoinduced crystalline habit change of a diarylethene derivative originated from anisotropic crystalline lattice changes caused by the isomerization of the molecules.[22] After such seminal works, a variety of studies on crystals and polymers with photomechanical effects have been reported.[32–35] Naumov's group intensively investigated crystals exhibiting a salient effect ("jump" of organic crystals) upon thermal or photoinduced crystalline structural changes.[36,37] Based on the comparison of the molecular arrangements before and after the crystalline jump, they proposed that only organic crystals showing martensitic phase transitions are salient active.[38]

Mechanical stimulation can induce changes in the crystal structure of solid materials.[39,40] Recently, studies of luminescent mechanochromic compounds have attracted attention where the color of a solid state emission can be switched by mechanical stimulation.[14–18] These color changes are caused by the mechano-induced crystalline structure changes in the materials that alter the intermolecular interaction patterns. Most of the reported crystalline mechanochromic luminescent materials show crystal to amorphous phase transitions (approximately 70%).[13,41–47] This is because the mechanical grinding or shearing is non-coherent and exerts random stimulation on the solid, which degrades the integrity of the materials. Indeed, mechano-triggered SCSC phase transitions have been seldom reported. However, some organic materials showing this type of SCSC phase transitions have been reported since 2013.[19,20,48,49] These examples may provide new insights that lead to understanding how macroscopic mechanical stimulation effectively changes microscopic molecular arrangements.

[a] Dr. T. Seki, K. Sakurada, M. Muromoto, Prof. Dr. H. Ito
Division of Applied Chemistry & Frontier Chemistry Center, Faculty of Engineering, Hokkaido University, Sapporo, Hokkaido 060-8628, Japan.
E-mail: hajito@eng.hokudai.ac.jp
[b] Prof. Dr. S. Seki
Department of Molecular Engineering, Graduate School of Engineering, Kyoto University, Kyoto 615-8510, Japan.
[c] Prof. Dr. S. Seki
Department of Applied Chemistry, Graduate School of Engineering, Osaka University, 2-1 Yamadaoka, Suita, Osaka 565-0871, Japan.

Supporting information for this article is available on the WWW under http://dx.doi.org/10.1002/chem.201303394.

We previously reported the SCSC phase transitions of the gold(I) isocyanide complexes **1**[19] and **2**[20] (Figure 1a), which were triggered by mechanical stimulation (Figure 1b). Rapid crystallization of **1** and **2** from a solution of dichloromethane/hexane gave blue- and green-emitting single crystals, of **1b** or **2g**, respectively. A small mechanical stimulation on a small area of a crystal of **1b** or **2g** readily showed a local area phase transition (left hand panels in Figure 1c and d). This phase transition then propagated over the entire crystal to give the daughter phases, $\mathbf{1y}_{scsc}$ and $\mathbf{2b}_{scsc}$, respectively (right hand panels in Figure 1c and d). It should be noted that the progression of the phase change on the crystal surfaces could be visualized by the change in the emission from blue to yellow (Figure 1c) and green to blue (Figure 1d).[50] X-ray diffraction analyses revealed that these phase transitions were SCSC, and gave a clear crystalline structural rationale for the emission color changes. **1** showed a red shift in the emission band because additional aurophilic interactions were formed.[15,19,51–57] In contrast, **2** exhibited a blue shift in the emission band, because a number of aurophilic interactions were disconnected.[20] Quite remarkably, these emission color changes in crystals of **1b** and **2g** could be initiated even by surface contact with $\mathbf{1y}_{scsc}$ and $\mathbf{2b}_{scsc}$ crystals, respectively.[19,20] The emission color of **1b** and **2g** at the contact point first started to change and this local phase transition propagated through the entire crystals in an SCSC manner. To the best of our knowledge, **1** and **2** are the first examples of SCSC phase transitions triggered by the mechanical stimulation and solid contact (solid seeding) at room temperature.[19,20,58]

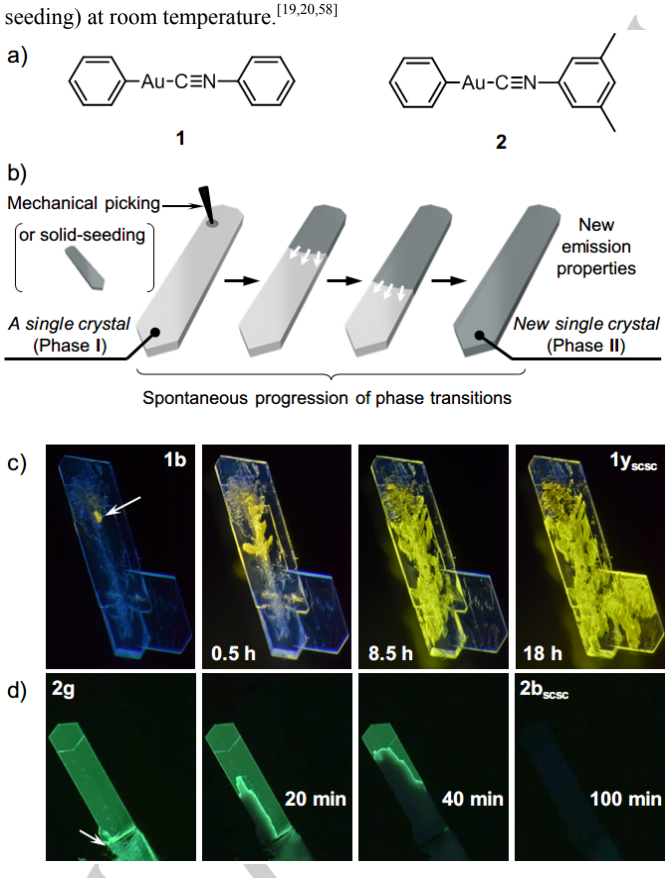

Figure 1. a) Structures of **1** and **2**. b) Schematic representation of the SCSC phase transition, triggered by mechanical picking and solid-seeding, that is accompanied by a photoluminescence color change. A series of photographs following the mechano-triggered SCSC phase transition of c) **1b** to $\mathbf{1y}_{scsc}$ and d) **2g** to $\mathbf{2b}_{scsc}$. The photographs were taken under ambient conditions with 365 nm illumination. The arrows in c) and d) indicate the area where the mechanical stimulation was applied.

With these two unique gold(I) complexes in hand, we conducted a series of comparative studies on the phase transitions. Herein, we report the detailed studies of **1** and **2**, including face index measurements of the mechano-triggered SCSC phase transition, thermal analyses, and electronic conductivity measurements. We first summarize the contrasting changing profiles of the emission properties and the crystal structural features (CH/π and Au···Au interactions) between **1** and **2** upon the mechano-triggered SCSC phase transitions. We next present the results of the face index measurements of the single crystals of **1** and **2** before and after the SCSC phase transitions to discuss how molecules move within the crystals. These studies revealed that the phase transitions of **1** and **2** proceeded through a nucleation and growth mechanism.[4,59] The thermal analyses of **1** and **2** showed they undergo exo- and endothermic polymorph transformations, respectively. The reason of this contrasting thermal behavior will be discussed in terms of the crystalline structures of **1** and **2**. We also investigate the electronic properties of **1** and **2** using a scanning electronic microscope (SEM) in charge transport sensitive conditions, and flash-photolysis time-resolved microwave conductivity (FP-TRMC)[60–63] measurements. These studies revealed that crystalline structures with more aurophilic interactions show superior electronic properties. Changes in the electronic properties of mechanochromic compounds have rarely been investigated. Finally, we will discuss an intriguing phenomenon of **2**, that of a *disappearing polymorphism*[5,64]

In Figure 2, we summarize the preparation of the luminescent polymorphs of **1** and **2**. For **1**, rapid and slow crystallization from the CH_2Cl_2/hexane gave blue- and yellow-emitting single crystals **1b** and **1y**, respectively (Figure 2a).[19] Upon applying external stimulation such as mechanical force, solid seeding, and thermal annealing to **1b**, the crystal undergoes an SCSC phase transition to give $\mathbf{1y}_{scsc}$. The crystal structures of **1y** and $\mathbf{1y}_{scsc}$ are identical. The preparation of the polymorphs of **2** is shown in Figure 2b.[20] Rapid crystallization afforded single crystals of **2g**. **2g** exhibited mechano-, solid-seeding-, and thermo-induced SCSC phase transition to give $\mathbf{2b}_{scsc}$. The crystal structure of $\mathbf{2b}_{scsc}$ is similar to that of **2b** which is obtained by slow crystallization of **2**. For both **1** and **2**, *intergrowth crystals,* in which two polymorph domains coexist in one crystal, can be obtained after applying a small mechanical stimulation and before completion of the phase transitions. We call these intergrowth crystals $\mathbf{1}_{IG}$ for **1** (Figure 2a) and $\mathbf{2}_{IG}$ for **2** (Figure 2b) and used them for evaluating the electronic properties by SEM.

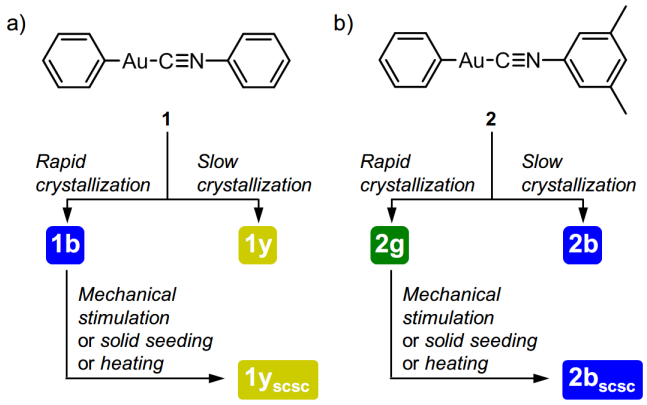

Figure 2. Molecular structures of **1** and **2** and the procedures for obtaining the different polymorphs.

Results and Discussion

Contrasting the Changes in the Photoluminescence and Crystalline Structures of 1 and 2

The most interesting aspect of the phase transition behaviors of **1** and **2** is the complementary change in the photoluminescence (Figure 3). Complex **1** crystallizes as the blue-emitting **1b** with emission maxima at 460 and 490 nm (black line in Figure 3a). After the SCSC phase transition of **1b** to **1y**$_{scsc}$ by mechanical stimulation, a structureless emission band was observed with a maximum at 566 nm (gray line in Figure 3a). This indicates that the SCSC phase transition of **1** induces a red-shift in the emission band (arrow in Figure 3a). Moreover, the absolute emission quantum yield Φ_{em} increased (4% → 16%) and the average emission lifetime τ_{av} was shortened (108 μs → 5.33 μs; Table S1). Complex **2** is different from **1** in only two methyl groups on the isocyanide phenyl moiety, but there are significant differences in the changes in the emission upon SCSC phase transition. Recrystallization of **2** from dichloromethane/hexane yields intensely green-emitting crystals of **2g**. The emission band of **2g** has a broad peak at 535 nm (black line in Figure 3b). Upon the mechano-triggered SCSC phase transition of **2g** to **2b**$_{scsc}$, the resulting crystal has a blue emission with Φ_{em} (84% → 6%) and lengthened τ_{av} (0.97 μs → 13.8 μs; Table S1). Gray line in Figure 3b indicates that mechano-triggered SCSC phase transition of **2** induces a blue shift to the emission band at 400–500 nm (arrow) with almost maintaining the original emission maximum around at 540 nm. Thus, **1** and **2** exhibit contrasting changes in their emission bands because of the phase transitions.

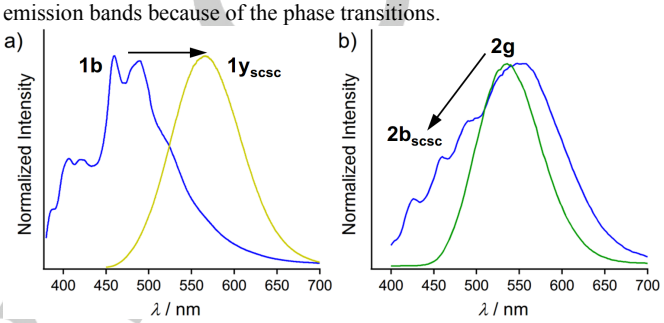

Figure 3. Emission spectra of a) **1b** (black line) and **1y** (gray line) normalized with maximum intensity and b) **2g** (black line) and **2b** (gray line) normalized with the corresponding maximum absorption intensities in which absorption spectra are not shown. Excitation wavelength is 365 nm.

The single crystal X-ray diffraction analyses unveiled the detailed molecular arrangements of **1** and **2** both before and after the phase transitions, which explain the changes in the emissions. The

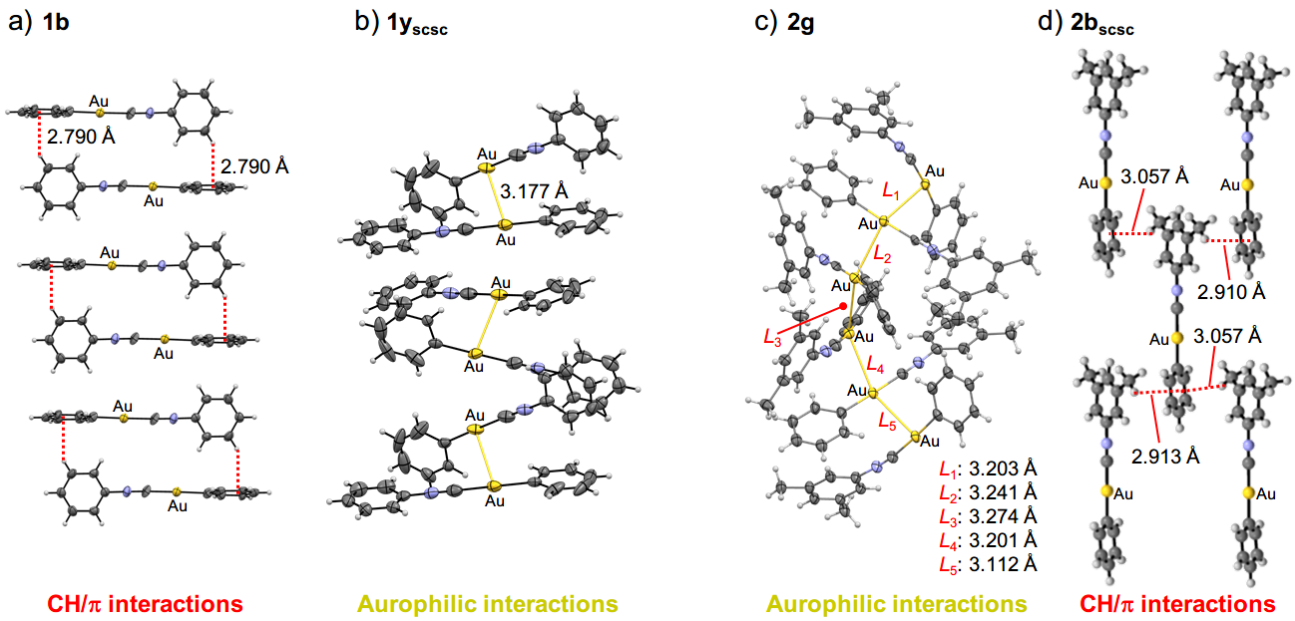

Figure 4. Crystal structures of a) **1b**, b) **1y**$_{scsc}$, c) **2g**, and d) **2b**$_{scsc}$. Dotted and solid lines denoted CH/π and aurophilic interactions, respectively. For more detailed crystallographic data, see the Supporting Information.

aurophilic interactions are the key to these changes. The SCSC phase transitions of **1** and **2** allow us to compare the crystalline structures in detail both before and after the phase transitions. Before the phase transition of **1**, **1b** crystallizes in the triclinic space group *P*-1 (Figure 4a and S1). Dimer units of **1** form through two CH/π interactions, which are further stacked to form one-dimensional columns via additional CH/π interactions. These columns packed to form a herringbone arrangement. The shortest inter-gold distance is 5.733 Å, indicating an absence of any aurophilic interactions. After the phase transition of **1b**, the space group of $\mathbf{1y}_{scsc}$ was the tetragonal *I*-42*d* (Figure 4b and S2). The molecules remain as dimers in 1-D columns with a head-to-tail orientation. Within the dimer unit however, aurophilic interactions with Au···Au distances of 3.177 Å have been formed. Comparing the crystal structures of **1b** and **1y** (Figure 4a and b, respectively) indicated that the phase transition of **1** is driven by the formation of these aurophilic interactions. It has been reported that aurophilic interactions, arising from the correlation and relativistic effects of Au atoms, have caused a reduction in the excitation energy level,[15,51–57] which is consistent with the red-shifted emission band of **1** (Figure 3a).

For **2**, the green-emitting **2g** crystalized in the monoclinic space group $P2_1/n$ (Figure 4c and S3). Aurophilic interactions, with an average Au···Au distance of 3.2064 Å, lead to the formation of hexamer units. These hexamers further stack to form 1-D columns along the direction of the *b*-axis through π–π stacking interactions. There is a void in the lattice of **2g** with a volume of 430.93 $Å^3$ per unit cell (5.2 v/v% of the unit cell). After the phase transition, the resulting weakly blue-emitting crystal of $\mathbf{2b}_{scsc}$ has an orthorhombic space group, *Ima*2 (Figure 4d and S4). All the molecules are oriented along the direction of the *b*-axis. The shortest Au···Au distance is 4.784 Å, which is too long to be an aurophilic interaction. Thus, this disconnection of aurophilic interactions is the most distinct feature; green-emitting **2g** with aurophilic interactions is transformed to blue-emitting **2b** that has CH/π interactions. Importantly, all the molecules in **2b** have four CH/π interactions. Comparisons of the crystalline structures of **2g** and **2b** (Figure 4c and d, respectively) indicated that the phase transition of **2** results in the disconnection of the aurophilic interactions, which reasonably explains the blue-shift in the emission band (Figure 3b).

Since the single crystal structure analyses of **1** and **2** before and even after the phase transitions (**1b**, $\mathbf{1y}_{scsc}$, **2g**, and $\mathbf{2b}_{scsc}$) were possible, we can unambiguously state that the contrasting changes in the photoluminescence of **1** and **2** are caused by the changes in their crystal structures (*i.e.*, the formation/cleavage of the aurophilic interactions; Figs S1–S4). Generally, all intermolecular interactions in the solid state can affect the optical and other related properties of the molecules. For gold complexes, however, aurophilic interactions often act a primary role to determine their molecular properties. This should hold true for our complexes. Again, successful single crystal X-ray diffraction analyses of the mechanically obtained phases (*i.e.*, $\mathbf{1y}_{scsc}$ and $\mathbf{2b}_{scsc}$) are rare and enable us to understand the origin of these emission color changes. By taking advantage of this intriguing feature of **1** and **2**, we further studied **1** and **2** in more detail on the phase transitions, thermal properties, and their electronic properties.

Face Indexing

Face index measurements of the crystals before and after the SCSC phase transitions may provide the information on how the molecules rearrange themselves inside the crystals. Propagation of the phase transitions of some molecular crystals are epitaxic when the two phases are structurally similar.[2,59] The epitaxic phase transitions exhibit rigorous orientational relationships between molecules in the mother and daughter phases, and this means face index measurements give the same results for each experiment. Molecular crystals with martensitic phase transitions, in which long-range atomic and molecular movement is negligible upon phase transition, can fall into this class. Compared with the minor crystal structure changes, some recently published organic molecular crystals show major packing changes upon thermal SCSC phase transition in which nucleation and elongation crystal growth are caused by the molecular rearrangement.[65] It is expected that face index measurements would afford different results for every experiment with those crystals due to the lack of rigorous relationship between mother and daughter phases.

The procedure for our face index measurements is shown schematically in Figure 5a. We first performed the face-indexing of **1b** and **2g** (*step i* in Figure 5a). The crystal was then unmounted from the Kapton loop (*step ii*) and mechanical stimulation was applied to a single area of the crystal by cutting off a small piece (*step iii*). After the phase transition was complete (*step iv*), the corresponding product crystals, $\mathbf{1y}_{scsc}$ and $\mathbf{2b}_{scsc}$, respectively, were remounted to the Kapton loop (*step v*) before being face indexed again (*step vi*). Photographs of the crystals before and after the face index experiments were shown in Figure 5b and S5 and S6.

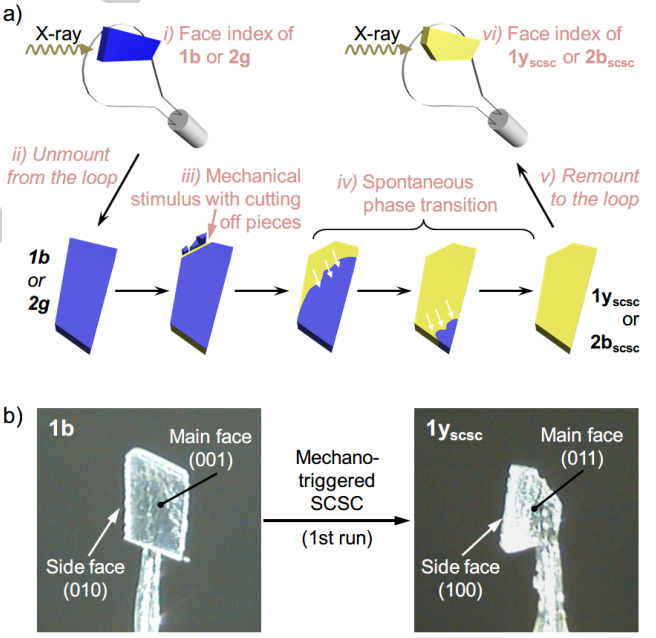

Figure 5. a) Schematic representation of the procedure used for the face index experiments of **1** and **2**. b) Photographs of the single crystals of **1b** and $\mathbf{1y}_{scsc}$ (taken under room light) which were used for the face indexing experiments through the mechano-triggered SCSC phase transitions (1st run). See the Supporting Information for the photographs of 2nd and 3rd run.

The face index experiments on three single crystals of **1b** prepared from the solution phase were conducted, providing essentially the same results (the left hand column in Table 1). Similar plate-like single crystals of **1b** were selected (the left hand panel in Figure 5b and S5). The major face of the three crystals was indexed as the (001) plane and the long side (second face) was indexed as the (010) plane (the left hand panel in Figure 5 and Figure 6a and c and the left hand column in Table 1). The reproducibility of the face index results of **1b** indicate that it crystallizes in the same relative orientation within the crystal, as is commonly observed.[66,67] The long axis of the 1-D stacked column in **1b** (see molecules represented by space-filling model in Figure 6a) is roughly perpendicular to the long axis of the crystal. Thus, the crystal grew preferentially almost perpendicular to the columns within the crystal.

Table 1. Results of the face index experiments on **1** before and after the mechano-triggered SCSC phase transition.

run	Faces of **1b** (step *i* in Figure 5a) major face/ its side		Faces of **1y**$_{scsc}$ (step *vi* in Figure 5a) major face/ its side
1st	(001) / (010)	→	(011) / (100)
2nd	(001) / (010)	→	(012) / (11$\bar{1}$)
3rd	(001) / (010)	→	(001) / (101)
Note	*Always same*		*Different each time*

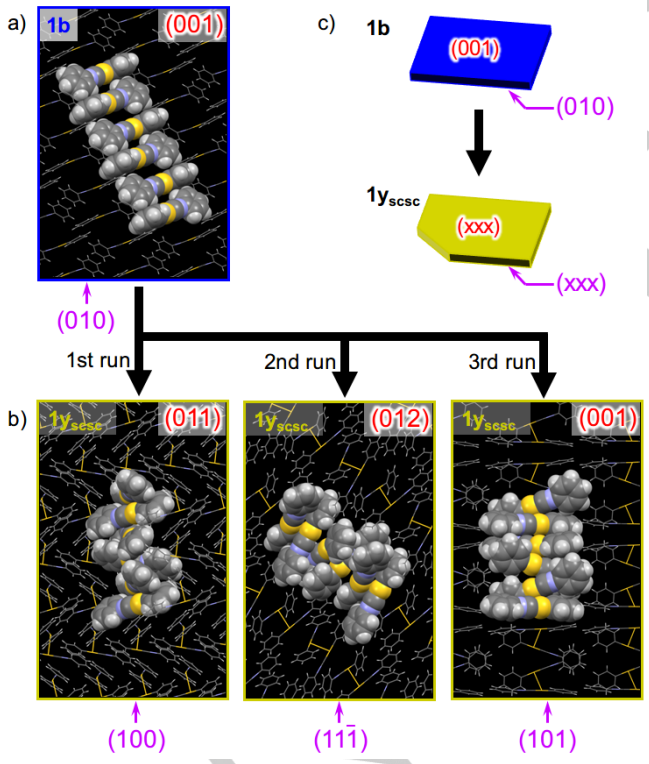

Figure 6. The results of the face index experiments on a) **1b** obtained by crystallization from solution and b) **1y**$_{scsc}$ obtained by mechano-induced SCSC phase transition from **1b**. Each crystal structure is shown perpendicular to the major faces. c) Schematic representations of the major (in red) and second faces (in purple).

The face index measurements on three single crystals of **2g** prepared by the recrystallization, again gave reproducible results (the left hand column in Table 2), similar to **1b**. The face index experiments of three plate-like single crystals of **2g** obtained from different batches gave the (010) plane as the major face, and the second face was the (100) plane (Figure 7a and c and the left hand column in Table 2). Similar to **1b**, the reproducibility of the face index results of **2g** indicates that this relative orientation in the crystal is favored. Further, it demonstrates that the crystalline growth of **2g** again occurred preferentially along the direction almost perpendicular to the 1-D columns containing multiple aurophilic interactions (see molecules represented by space-filling model in Figure 7a). Unlike **1b**, **2g** has multiple CH/π interactions between columns parallel to the long axis of the crystal that presumably play a role in the growth along this axis. This differs from Slauter's work in which a crystal of a platinum isocyanide complex preferentially grows along the axis of the Pt···Pt bonds.[67]

Table 2. Results of the face index experiments on **2** before and after the mechano-triggered SCSC phase transition.

run	Faces of **2g** (step *i* in Figure 5a) major face/ its side		Faces of **2b**$_{scsc}$ (step *vi* in Figure 5a) major face/ its side
1st	(010) / (100)	→	($\bar{1}$10) / ($\bar{0}\bar{1}$1)
2nd	(010) / (100)	→	(10$\bar{1}$) / (010)
3rd	(010) / (100)	→	(100) / (010)
Note	*Always same*		*Different each time*

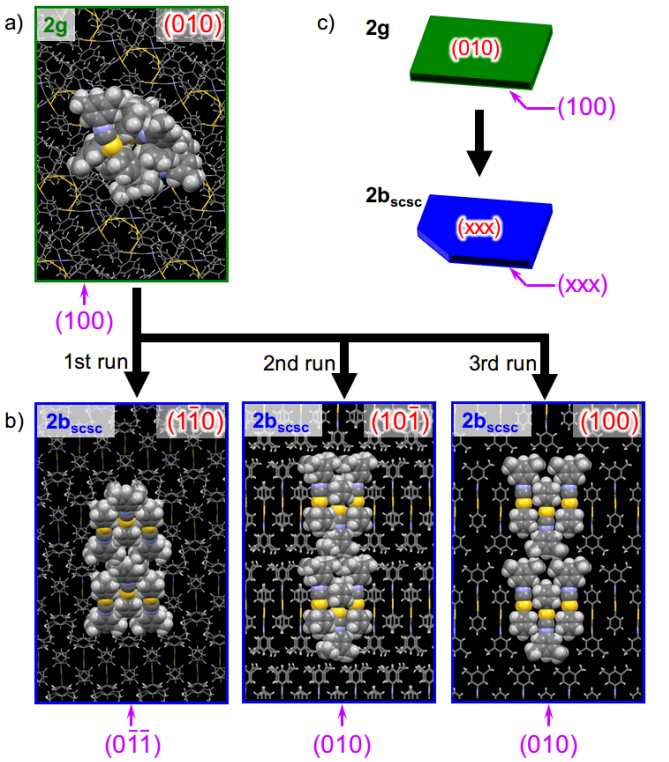

Figure 7. The results of the face index experiments of a) **2g** obtained by crystallization from solution phase and b) **2b**$_{scsc}$ obtained by mechano-induced SCSC phase transition. All these crystal structures are viewed perpendicular to the major faces. c) Schematic representations of the major (red letters) and second faces (purple letters).

For the product phases of **1** and **2**, **1y**$_{scsc}$ and **2b**$_{scsc}$, respectively, the results of the face index experiments varied depending on the crystals measured (the right hand columns in Tables 1 and 2). Based on the face index measurements of three crystals of **1y**$_{scsc}$ obtained from **1b** (Figure 5a), the major and second faces indexed differently for each crystal (Figure 6b and c and S5 and the right hand column in Table 1). It should be noted that these **1y**$_{scsc}$ crystals were obtained from **1b** crystals that gave consistent face index results (Table 1). In the face index measurements of the product phases of **2** (**2b**$_{scsc}$), the major and second faces were also indexed differently for each crystal (Figure 7b and c and S6 and the right hand column in Table 2). Moreover, when **1y**$_{scsc}$ and **2b**$_{scsc}$ are obtained by thermal annealing of **1b** and **2g**, respectively, the face indexing measurements yielded similar results:[68] the relative direction of the crystallographic axes in the product crystals (**1y**$_{scsc}$ and **2b**$_{scsc}$) are different for each crystal (Figure S7 and S8, respectively).

The face index measurements of **1y** and **2b**, which were prepared by slow crystallization from the solutions of **1** and **2** (Figure 2), were also conducted. By slow crystallization from solutions at room temperature (*i.e.*, >12 h), the thermodynamically favored **1y** and **2b** are reproducibly formed as single crystals (Figure 2).[19,20] The internal crystal structures of these crystals are identical to those of **1y**$_{scsc}$ and **2b**$_{scsc}$, respectively. However, the results of the face index measurements on **1y** and **1y**$_{scsc}$ and **2b** and **2b**$_{scsc}$ are different. **1y** crystallizes with an octahedral habit, rather than as platelets. Three highly symmetric crystals of **1y** gave reproducible face index results (Figure S9). This contrasts with the face index experiments of **1y**$_{scsc}$ obtained by the SCSC phase transition of **1b** (the right hand column in Table 1) which gave different results for each crystal. Similarly, the three plate like crystals of **2b** obtained by slow crystallization, gave reproducible face-indexing, with the major face corresponding to the (001) plane and the second face to the (010) plane (Figure S10).[69]

These results mean that there is no rigorous orientation relationship between the mother and daughter phases of the mechano-triggered phase transitions. In other words, the SCSC phase transitions of **1** and **2** are not based on epitaxial phase transitions.[2,59] We propose that a nucleation and crystal growth mechanism is involved in the SCSC phase transitions of **1** and **2**. This is because of the large differences in the packing arrangements before and after the phase transitions as well as the "random orientation" of **1y**$_{scsc}$ and **2b**$_{scsc}$. In the case of the phase transition of *p*-dichrobenzene crystal, such randomly oriented molecular rearrangement was reported in which crystalline structures of the mother and daughter phases are quite different.[59] In general, SCSC phase transitions occur between crystalline arrangements with only minor structural differences.[8,22,48,67,70–73] Minor structural differences mean the molecular movements in the mother phase are small in the transformation to the daughter phase allowing the phase transition to occur epitaxially.[1] On the other hand, the molecular arrangements of **1b**/**1y**$_{scsc}$ and **2g**/**2b**$_{scsc}$ are dramatically different (Figure 4), and thus these complexes do not show an epitaxial phase transitions and result in a "random orientation" of the daughter phases **1y**$_{scsc}$ and **2b**$_{scsc}$.

A schematic explanation of the crystal phase diversity is shown in Figure 8. A small initial nucleus is generated by the small mechanical stimulation on the crystal surface of **1b** and **2g**. The phase development from the nuclei is rapid enough that the daughter phase spreading from the one nucleus predominates, causing a single orientation to be observed after the completed phase conversion. The crystal orientation of the initial nuclei would be different for each experiment, which corresponds to the different face index results shown in Tables 1 and 2.[74] Although the nucleation and crystal growth mechanism of the phase transitions observed in **1** and **2** is rare even in a thermal phase transition, the group of Sureshan recently reported the thermal SCSC phase transition of 4,6-*O*-benzylidene-*α*-*D*-galactosyl azide occurs through a nucleation and crystal growth mechanism with major packing changes.[65]

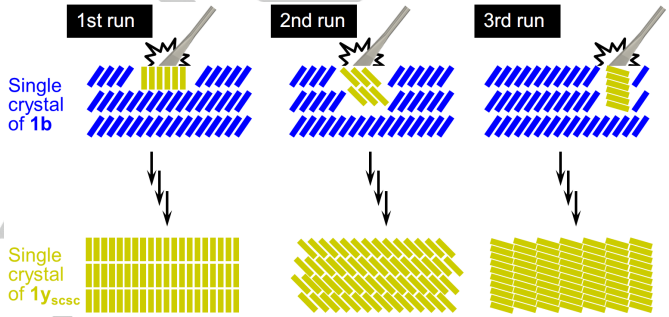

Figure 8. Schematic representation of the results from the face index experiments of the mechano-triggered SCSC phase transition of **1b** to **1y**$_{scsc}$. Black and gray rectangles denoted molecules **1** in the crystalline lattice of **1b** and **1y**$_{scsc}$, respectively. Relative molecular orientations in the resulting **1y**$_{scsc}$ crystals (bottom) are determined by the molecular orientations first generated by the mechanical stimulation of the **1b** crystalline domains (top).

Thermal Properties

The thermal phase transitions of **1** and **2** have been evaluated by DSC analyses and microscopic observation. Upon heating pristine crystals of **1b** at a rate of 5 °C min^{-1}, exothermic peaks are observed between 60 and 80 °C (Figure 9a). Together with the emission color change (Figure 9b), these exothermic peaks can be attributed to an enthalpically driven phase transition to a yellow-emitting polymorph (such as **1y**). We have previously reported on the thermal SCSC phase transition of **1b** to **1y**$_{scsc}$.[19] Three DSC measurements of **1b** indicate the enthalpic change of this phase transition is approximately −7 kJ/mol.[75] The DSC profile of **1y** (obtained by recrystallization) has no discernible peaks until an endothermic peak at 130 °C (due to melting), indicating the absence of the phase transition (Figure 9a).[76] This is consistent with the absence of a thermal induced emission color change in **1y** (Figure 9b). These thermal experiments represent the lower Gibbs free energy of **1y** than **1b**, and enthalpy changes originated from the newly formed aurophilic bonds would be the principal contribution to this thermodynamic gain.

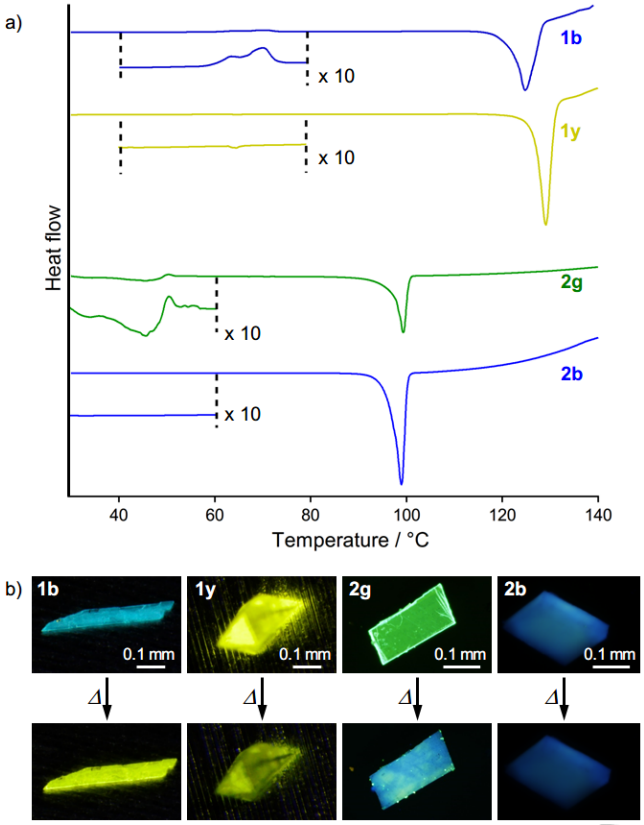

Figure 9. a) DSC profiles of **1b**, **1y**, **2g**, and **2b** at a heating rate of 5 °C min^{-1}. b) Photographs of **1b**, **1y**, **2g**, and **2b** at 25 °C (top) and the corresponding photographs at higher temperature (bottom, 80°C for **1b** and **1y**; 50°C for **2g** and **2b**). The absence of emission color change of **1y** and **2b** upon heating indicates that no thermal phase transition has occurred.

Figure 9a also shows the DSC profiles of **2**. The DSC profile of **2g** shows a small and broad endothermic peak around 50 °C (Figure 9a), indicating the phase transition of **2g** to **2b**. Three DSC measurements of **2g** indicate the enthalpic change of this phase transition is approximately +5 kJ/mol. This transformation is supported by the change in the emission color of **2g** from green to blue at 50 °C (Figure 9b). Moreover, the endothermic peak indicates that **2g** undergoes an entropically driven phase transition to the thermodynamically favorable **2b**.[77] This is different from complex **1**. In contrast, **2b** has a featureless DSC profile (Figure 9a) and does not change emission color at 50 °C (Figure 9b). These thermal analyses indicate that the **2b** phase has a lower Gibbs free energy than **2g**, even though **2b** has a higher enthalpic energy than **2g**.

It has been suggested that difference in the exo- and endothermic phase transitions of **1** and **2** can be explained in terms of their crystal structures. Recently, thermal SCSC phase transitions of a series of naphthyridine compounds with slight differences in the substituents, exhibited exo-[6] and endothermic[78] thermal phase transitions. In these reports, the origin of the difference in the thermal behaviors between these two different naphthyridines was not discussed, but in practice the source of the difference is hard to determine. Indeed, this difference in these phase transitions of **1** and **2**, is not fully understood at present, but our tentative explanation is as follows. The exothermic phase transition from **1b** to $\mathbf{1y}_{scsc}$ comes from the formation of the aurophilic interactions, whose strength is relatively high as an intermolecular interaction, being comparable to that of hydrogen bonds.[15,51–57] For **2**, an endothermic phase transition was observed from **2g** into $\mathbf{2b}_{scsc}$. We suppose that the relatively large negative change in the enthalpy on the disconnection of the aurophilic bonds in **2g** can be partially compensated by the formation of multiple CH/π interactions of $\mathbf{2b}_{scsc}$. The phase transition from **2g** to **2b** is entropically favorable because the empty void region in the mother phase **2g** (5.2 v/v%) has collapsed in the daughter phase **2b** (0 v/v%).[20] In both cases, the daughter phases of **1** and **2** are favorable in terms of Gibbs free energy and thus, domino like SCSC phase transitions take place under ambient conditions when local mechanical stimulation is applied.

Scanning Electron Microscopy of the Intergrowth Crystals

We prepared *intergrowth crystals*[79] of **1** and **2**, referred to as $\mathbf{1}_{IG}$ and $\mathbf{2}_{IG}$, respectively and the electronic properties of the polymorphs of these complexes were investigated (Figure 10). Intergrowth crystals contain multiple crystal domains of different polymorphs. Because the mechano-triggered SCSC phase transition of **1** and **2** take some several tens of minutes, $\mathbf{1}_{IG}$ and $\mathbf{2}_{IG}$ can be observed after applying the small mechanical stimulation and before completion of the phase transitions. Because the different phases have distinct emission properties, the formation of intergrowth crystals of $\mathbf{1}_{IG}$ and $\mathbf{2}_{IG}$ can be characterized based on the two different emissions from one crystal (Figure 10a and c, respectively).[79] Indeed, the microscopic photoluminescence measurements of $\mathbf{1}_{IG}$ and $\mathbf{2}_{IG}$ showed that the emission spectra of the two domains in the same crystal are very similar to those of the corresponding pure polymorphs (Figure S11), confirming their intergrowth nature. Generally, the preparation of the intergrowth crystals with physically distinct polymorph domains, is hard to achieve by crystallization,[79] because different polymorphs generally crystallized independently (*i.e.*, *concomitant polymorphism*[1,3,4]).

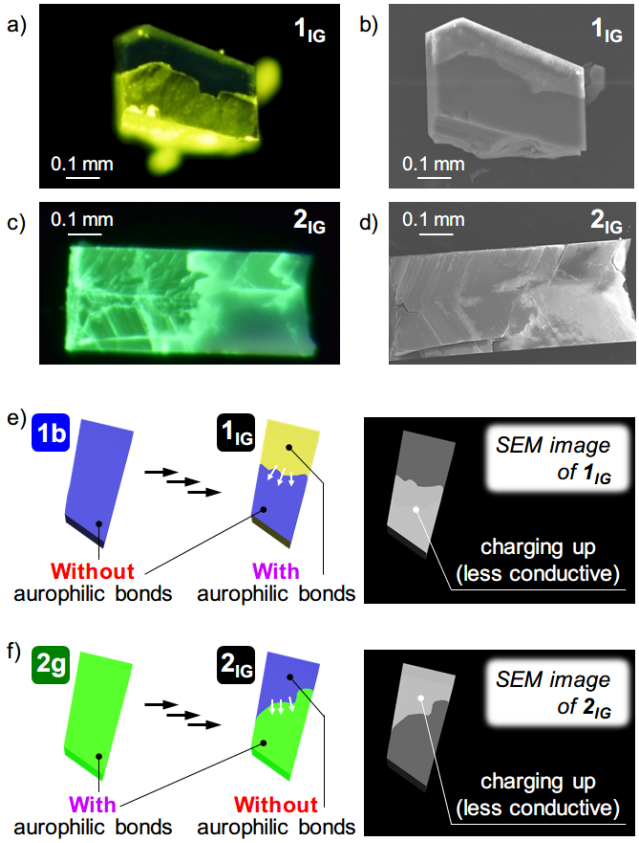

Figure 10. Photoluminescence microscope images of a) $\mathbf{1}_{IG}$ and c) $\mathbf{2}_{IG}$ under excitation at 365 nm and b) sputtering-free SEM images of b) $\mathbf{1}_{IG}$ and d) of $\mathbf{2}_{IG}$. Schematic representations of charging in $\mathbf{1}_{IG}$ e) and $\mathbf{2}_{IG}$ f), when observed by SEM.

We next observed $\mathbf{1}_{IG}$ and $\mathbf{2}_{IG}$ by SEM without metal sputtering prior to the measurements. Because two polymorph domains coexist in one crystal of $\mathbf{1}_{IG}$ and $\mathbf{2}_{IG}$, the differences in the properties of the polymorphs, such as electronic properties, can be compared under identical experimental conditions.[1,80–83] Figure 10b shows an SEM image of $\mathbf{1}_{IG}$ obtained after the sample was placed onto the conductive carbon sheet, which has two different polymorph domains. The domain of the upper half of the crystal, corresponding to the **1b** domain, looks whitish probably due to charging. In SEM measurements, accelerated electrons often induce charging up of specimens via nocking-out of secondary electrons with electric insulating nature (*i.e.*, organic compounds) when their surfaces are not overcoated with conductive metals.[84] As a result, typical whitish, low contrast sample images are obtained. The **1y** domain (on the bottom half of the crystal in Figure 10b), however, does not show a significant charging effect. This suggests that the **1b** domain has conductive pathways for charge carriers injected into domain. In Figure 10d, the SEM image of $\mathbf{2}_{IG}$ shows the charging effect more significant in the **2b** domain (right half of the crystal domain), whereas **2g** on the left hand side shows much less charging (Figure 10d). This indicates that as-prepared, unchanged crystalline domain **2g** has the greater charge conductive pathways.

These SEM observation of $\mathbf{1}_{IG}$ and $\mathbf{2}_{IG}$ revealed that the aurophilic interactions in the crystalline lattice[15,51–57,85] reverse conductive pathways for charge carriers in **1** and **2** because of the observed decrease in charging (Figure 10e and f). Generally, strong intermolecular interactions and ordered molecular arrangements improve electronic coupling between adjacent molecules, which often leads the higher charge carrier mobility. One such strong intermolecular interaction found in the crystal lattices of **1** and **2** is the aurophilic interaction.[15,51–57] The crystal lattices, **1y** and **2g**, which contain the aurophilic interactions (Figure 4b and c, respectively) show less charging, and this suggests these interactions improve the electronic coupling in this system. Interestingly, the **1y** domain of $\mathbf{1}_{IG}$ exhibited a decrease in charging (Figure 10a), indicating the rearrangement of highly conductive pathways after the phase transition. Generally, phase transitions decrease crystal quality which should divide the pathways, but this effect is less prominent for the **1y** domain, as evidenced by the less prominent charging effect after the transition.[82,83]

Electronic Conductivity Measurements

To increase our knowledge of the electronic properties of the polymorphs of **1** and **2**, flash-photolysis time resolved microwave conductivity (FP-TRMC) measurements were carried out. Evaluation of the conducting properties of samples generally requires contacting electrodes.[60–63] For our compounds, that direct contact of the electrodes on the crystal surfaces could induce a phase change, which would cause imprecise evaluation of the electronic conductivity. FP-TRMC is a non-contacting method for electronic conductivity measurements, providing an ideal method for our mechanically sensitive samples. Because short-range (approximately 10 nm) intrinsic conductivity can be estimated by FP-TRMC measurements, we can evaluate the conductivity of the crystalline materials that reflects their molecular packing arrangements and the intermolecular interaction patterns rather than the crystal size, habit, and other macroscopic features (i.e., defects).

Figure 11a shows the TRMC signals of **1b** and **1y**. For the FP-TRMC measurements, crystals of **1b** and **1y** were dispersed in a polyvinyl alcohol (PVA) polymer matrix which is expected to prevent degradation of the crystal samples upon laser irradiation. Upon the laser excitation of these complexes (Nd:YAG laser, λ_{ex} = 355 nm), a sharp onset appeared and the conductivity is gradually decreased. The maximum transient conductivity of **1b** was $\phi\Sigma\mu = 1.3 \times 10^{-5}$ cm^2 V^{-1} s^{-1} based on the end-of-pulse conductive profile (black line in Figure 11a). The conductivity of **1y** was significantly higher at $\phi\Sigma\mu = 1.3 \times 10^{-4}$ cm^2 V^{-1} s^{-1} (gray line in Figure 11a).[88] The superior TRMC performance of **1y** is in line with the SEM observations of $\mathbf{1}_{IG}$, where the **1b** domain showed charging and the **1y** domain showed less (Figure 10b and e). These results indicate that when the phase transition of **1** occurs due to a small mechanical stimulation or thermal treatment, its conductive properties are enhanced. Most likely, the increased conductivity of **1** can be attributed to the formation of aurophilic interactions (Figure 4a and b).

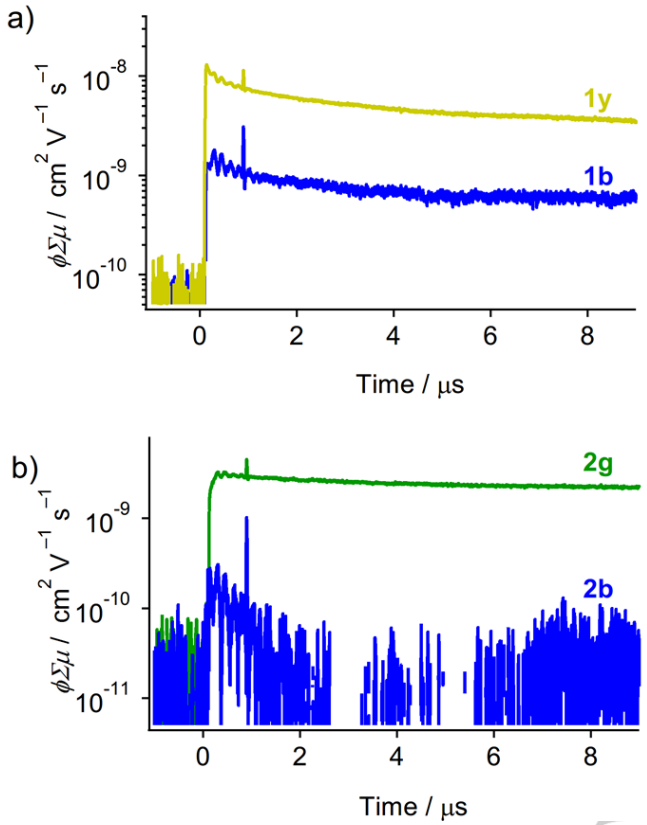

Figure 11. a) FP-TRMC transient signals for **1b** (black line) and **1y** (gray line) at room temperature. b) FP-TRMC transient signals for **2g** (black line) and **2b** (gray line) at room temperature.

Figure 11b shows the TRMC signals of **2g** (black line) and **2b** (gray line). The maximum transient conductivities of **2g** and **2b** are 3.2 × 10^{-5} and 2.8 × 10^{-6} cm^2 V^{-1} s^{-1}, respectively. Therefore, the conductivity of **2g** is approximately one order of magnitude greater than **2b**. Therefore, unlike complex **1**, the thermodynamically stable form **2b** is less conductive. This is again consistent with the results of the SEM observation (Figure 10d and f) and attributable to changes in the aurophilic interactions of **2g** and **2b**. Therefore, the difference in the conductivity is attributable to the presence/absence of the aurophilic interactions of **2g** and **2b**.

Disappearing Polymorph of 2

During this study, we encountered a "disappearing polymorph phenomena" in complex **2**. It has been reported that some polymorph forms cannot be obtained after some period of time even though they were easily obtained earlier on. This phenomenon is called *disappearing polymorphism*,[5,64,89–92] and is quite problematic in polymorphic compounds, especially in the pharmaceutical industry.[93] In 2012, we could obtain an orange-emitting polymorph of **2**, named **2o**, by a thermal phase transition of **2g** at 55 °C for 120 s (Figure 12a). After one month, we could not obtain the **2o** phase any more, even after repeated trials in various conditions. Instead, the thermal treatment of **2g** always afforded the **2b**$_{scsc}$ phase as we reported in the previous communication[20] and this present study.[94] Therefore, the **2o** polymorph form has *disappeared*.

Because the phase transition of **2g** to **2o** proceeded in an SCSC manner, we obtained a single crystal structure analysis of **2o** of suitable quality. **2o** forms in the monoclinic space group $P2_1/n$ [R_1 = 5.51%, wR_2 = 14.27%, GOF = 0.962, a = 17.7933(6) Å, b = 24.0917(7) Å, c = 20.1710(7) Å, $\alpha = \gamma = 90°$, β = 110.2310(9)°, Z = 24, V = 8113.3(5) Å^3, d = 1.990 g·cm^{-3}] (Figure 12c and Table S2). We found that the crystal structure of **2o** is very similar to that of **2g** (Figure 12b and c). For example, the space group is the same, both crystals have the particularly large unit cells (V > 8000 Å^3, Z = 24) and the overall crystal structures are quite similar (Figure 12b and c, Figure S3 and S13, and Table S2). The molecules in **2o** form hexamers that are connected together through intermolecular aurophilic interactions with an average distance of 3.0816 Å (Figure 12c). This average distance between the Au atoms of the hexamer is shorter than that of **2g** (3.2064 Å, Figure 12b). Thus, the stronger aurophilic bonds of **2o** are responsible for the different optical properties. The emission spectrum of **2o** upon the excitation at 365 nm showed a structureless emission band with a peak at 615 nm (Figure S14). This is a longer wavelength emission than in **2g** ($\lambda_{em,max}$ = 535 nm). Unfortunately, we cannot measure other photophysical properties of **2o** such as τ_{av} and Φ_{em} because we could not prepare this polymorph again. The crucial difference in the crystal structures of **2g** and **2o** is the volume of the void: the former is 5.2 % and the latter is only 0.5%. We believe that decreasing the void region by a small conformational change is the driving force for this phase transition (**2g** → **2o**). Again, it is unclear why the **2o** phase could not be found again as is the case of other disappearing polymorphs.[5,64,89–92]

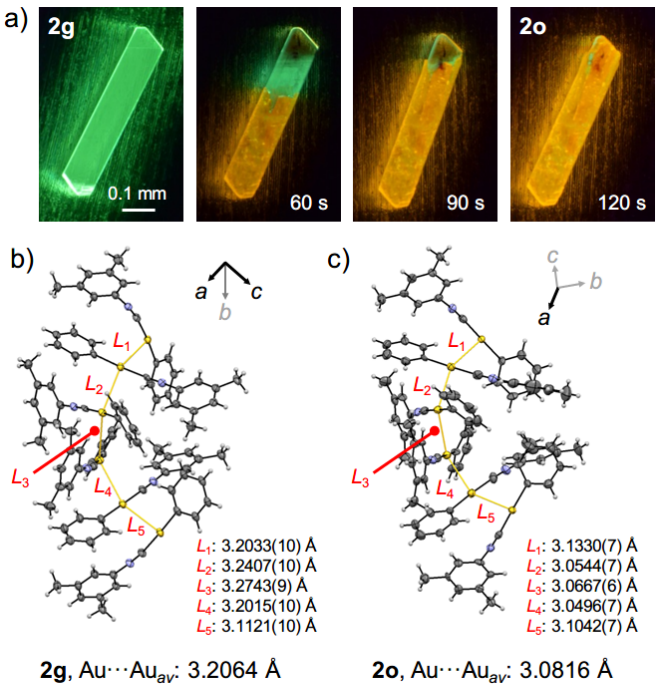

Figure 12. a) A series of photographs showing the thermal SCSC phase transition of **2g** to **2o** at 55°C. The photographs were taken under the ambient conditions and 365-nm illumination. ORTEP representations of the hexamer unit of b) **2g** and c) **2o** showing the multiple intermolecular aurophilic interactions.

WILEY-VCH

Summary

We studied the gold(I) isocyanide complexes **1** and **2**, which exhibit a particularly intriguing mechano-triggered SCSC phase transition. The face index measurements revealed that the mechano- and thermal induced phase changes of these two complexes proceeded through a nucleation and crystal growth mechanism rather than epitaxial phase transition process. The initially formed crystalline domain within the mother phase determines the relative orientation of the molecules in the daughter phase. Thus, there is no rigorous orientational relationship between the molecules in mother and daughter phases. DSC analyses of **1** and **2** revealed they have exo- and endothermic phase transitions, respectively. The phase transition of **1** is enthalpically driven because of the formation of aurophilic interactions, whereas **2** is entropically driven because of the closure of an empty void region. These contrasting thermodynamic properties attributed to the difference in the crystal structures. We also investigated the electronic properties of **1** and **2** by means of SEM observation and FP-TRMC methods. The charging observed during SEM measurements of **1** and **2** suggests that the polymorphs that include aurophilic interactions exhibit superior electronic conductivity. This was further confirmed by the FP-TRMC measurements of these complexes. We also reported a disappearing polymorph of complex **2**. The present studies provide useful information of polymorphic materials because all crystalline phases could be characterized by single crystal X-ray diffraction. Future studies will focus on the molecular arrangements and the properties of the intermediate phases in these systems. Such careful analyses may further our understanding of why macroscopic mechanical stimulation can effectively affect microscopic molecular arrangement.

Acknowledgements

This work was financially supported by the MEXT (Japan) program "Strategic Molecular and Materials Chemistry through Innovative Coupling Reactions" of Hokkaido University, and JSPS KAKENHI Grant-in-Aid for Scientific Research (B) 15H03804; and JSPS KAKENHI Grant-in-Aid for Challenging Exploratory Research, 26620053 and 15K13633 and for Young Scientists (B), 26810042. We also thank the support of Frontier Chemistry Center Akira Suzuki "Laboratories for Future Creation" Project, Hokkaido University.

Keywords: phase transition · single crystal · photoluminescence · mechanical stimulation · gold(I) complex

[1] J. Bernstein, R. J. Davey, J. O. Henck, *Angew. Chem. Int. Ed.* **1999**, *38*, 3440–3461.

[2] Y. Mnyukh, *Fundamentals of Solid-State Phase Transitions: Ferromagnetism and Ferroelectricity*; Authorhouse, 2001.

[3] R. Hilfiker, *Polymorphism in the Pharmaceutical Industry*; Wiley-VCH: Weinheim, 2006.

[4] A. Laguna, *Modern Supramolecular Gold Chemistry: Gold–Metal Interactions and Applications*; Wiley-VCH; John Wiley distributor: Weinheim Chichester, 2008.

[5] G. R. Desiraju, J. J. Vittal, A. Ramanan, *Crystal Engineering: a Textbook*; World Scientific; IISc Press: New Jersey, N. J., 2011.

[6] Y. Abe, S. Karasawa, N. Koga, *Chem. Eur. J.* **2012**, *18*, 15038–15048.

[7] N. Harada, S. Karasawa, T. Matsumoto, N. Koga, *Cryst. Growth Des.* **2013**, *13*, 4705–4713.

[8] T. Seki, K. Sakurada, M. Muromoto, H. Ito, *Chem. Sci.* **2015**, *6*, 1491–1497.

[9] J. C. Vickery, M. M. Olmstead, E. Y. Fung, A. L. Balch, *Angew. Chem. Int. Ed.* **1997**, *36*, 1179–1181.

[10] M. Kato, *Bull. Chem. Soc. Jpn.* **2007**, *80*, 287–294.

[11] M. Chang, A. Kobayashi, K. Nakajima, H. C. Chang, M. Kato, *Inorg. Chem.* **2011**, *50*, 8308–8317.

[12] O. S. Wenger, *Chem. Rev.* **2013**, *113*, 3686–3733.

[13] S. H. Lim, M. M. Olmstead, A. L. Balch, *Chem. Sci.* **2013**, *4*, 311–318.

[14] Y. Sagara, T. Kato, *Nat. Chem.* **2009**, ***1***, 605–610.

[15] A. L. Balch, *Angew. Chem. Int. Ed.* **2009**, *48*, 2641–2644.

[16] Z. Chi, X. Zhang, B. Xu, X. Zhou, C. Ma, Y. Zhang, S. Liu, J. Xu, *Chem. Soc. Rev.* **2012**, *41*, 3878–3896.

[17] X. Zhang, Z. Chi, Y. Zhang, S. Liu, J. Xu, *J. Mater. Chem. C* **2013**, *1*, 3376–3390.

[18] C. Jobbágy, A. Deák, *Eur. J. Inorg. Chem.* **2014**, *2014*, 4434–4449.

[19] H. Ito, M. Muromoto, S. Kurenuma, S. Ishizaka, N. Kitamura, H. Sato, T. Seki, *Nat. Commun.* **2013**, *4*, 2009.

[20] T. Seki, K. Sakurada, H. Ito, *Angew. Chem. Int. Ed.* **2013**, *52*, 12828–12832.

[21] Q. Chu, D. C. Swenson, L. R. MacGillivray, *Angew. Chem. Int. Ed.* **2005**, *44*, 3569–3572.

[22] S. Kobatake, S. Takami, H. Muto, T. Ishikawa, M. Irie, *Nature* **2007**, *446*, 778–781.

[23] L. R. MacGillivray, G. S. Papaefstathiou, T. Friščić, T. D. Hamilton, D. K. Bučar, Q. Chu, D. B. Varshney, I. G. Georgiev, *Acc. Chem. Res.* **2008**, *41*, 280–291.

[24] Z. Huang, P. S. White, Brookhart, M. *Nature* **2010**, *465*, 598–601.

[25] O. V. Zenkina, E. C. Keske, R. Wang, C. M. Crudden, *Angew. Chem. Int. Ed.* **2011**, *50*, 8100–8104.

[26] B. Manna, A. K. Chaudhari, B. Joarder, A. Karmakar, S. K Ghosh, *Angew. Chem. Int. Ed.* **2012**, *52*, 998–1002.

[27] I. H. Park, S. S. Lee, J. J. Vittal, *Chem. Eur. J.* **2013**, *19*, 2695–2702.

[28] G. D. Zou, G. G. Zhang, B. Hu, J. R. Li, M. L. Feng, X. C. Wang, X. Y. Huang, *Chem. Eur. J.* **2013**, *19*, 15396–15403.

[29] G. K. Kole, T. Kojima, M. Kawano, J. J. Vittal, *Angew. Chem. Int. Ed.* **2014**, *53*, 2143–2146.

[30] I. H. Park, A. Chanthapally, Z. Zhang, S. S. Lee, M. J. Zaworotko, J. J. Vittal, *Angew. Chem. Int. Ed.* **2014**, *53*, 414–419.

[31] B. C. Tzeng, A. Chao, *Chem. Eur. J.* **2015**, *21*, 2083–2089.

[32] O. S. Bushuyev, A. Tomberg, T. Friščić, C. J. Barrett, *J. Am. Chem. Soc.* **2013**, *135*, 12556–12559.

[33] Z. Jiang, M. Xu, F. Li, Y. Yu, *J. Am. Chem. Soc.* **2013**, *135*, 16446–16453.

[34] Y. Matsunaga, K. Goto, K. Kubono, K. Sako, T. Shinmyozu, *Chem. Eur. J.* **2014**, *20*, 7309–7316.

[35] T. Kim, L. Zhu, L. J. Mueller, C. J. Bardeen, *J. Am. Chem. Soc.* **2014**, *136*, 6617–6625.

[36] S. C. Sahoo, M. K. Panda, N. K. Nath, P. Naumov, *J. Am. Chem. Soc.* **2013**, *135*, 12241–12251.

[37] N. K. Nath, M. K. Panda, S. C. Sahoo, P. Naumov, *CrystEngComm* **2014**, *16*, 1850–1858.

[38] For one example of salient effect induced by photoirradiation, see: P. Naumov, S. C. Sahoo, B. A. Zakharov, E. V. Boldyreva, *Angew. Chem. Int. Ed.* **2013**, *52*, 9990–9995. See also reference [3].

[39] M. M. Caruso, D. A. Davis, Q. Shen, S. A. Odom, N. R. Sottos, S. R. White, J. S. Moore, *Chem. Rev.* **2009**, *109*, 5755–5798.

[40] P. A. May, J. S. Moore, *Chem. Soc. Rev.* **2013**, *42*, 7497–7506.

[41] H. Ito, T. Saito, N. Oshima, N. Kitamura, S. Ishizaka, Y. Hinatsu, M. Wakeshima, M. Kato, K. Tsuge, M. Sawamura, *J. Am. Chem. Soc.* **2008**, *130*, 10044–10045.

[42] N. D. Nguyen, G. Zhang, J. Lu, A. E. Sherman, C. L. Fraser, *J. Mater. Chem.* **2011**, *21*, 8409–8415.

[43] K. Kawaguchi, T. Seki, T. Karatsu, A. Kitamura, H. Ito, S. Yagai, *Chem. Commun*. **2013**, *49*, 11391–11393.

WILEY-VCH

[44] Z. Ma, M. Teng, Z. Wang, S. Yang, X. Jia, *Angew. Chem. Int. Ed.* **2013**, *52*, 12268–12272.

[45] H. Sun, S. Liu, W. Lin, K. Y. Zhang, W. Lv, X. Huang, F. Huo, H. Yang, G. Jenkins, Q. Zhao, W. Huang, *Nat. Commun.* **2014**, *5*, 3601.

[46] W. Li, L. Wang, J.-P. Zhang, H. Wang, *J. Mater. Chem. C* **2014**, *2*, 1887–1892.

[47] M. S. Kwon, J. Gierschner, J. Seo, S. Y. Park, *J. Mater. Chem. C* **2014**, *2*, 2552–2557.

[48] G. Liu, J. Liu, Y. Liu, X. Tao, *J. Am. Chem. Soc.* **2014**, *136*, 590–593.

[49] Recently, Takamizawa reported that the mechano-triggered SCSC phase transition of an organic molecule induces "superelastic" behavior: S. Takamizawa, Y. Miyamoto, *Angew. Chem. Int. Ed.* **2014**, *53*, 6970–6973.

[50] For complex **2**, the movies for the mechano- and solid-contact-induced phase transitions are available. See reference [20].

[51] A. L. Balch, *Gold Bull.* **2004**, *37*, 45–50.

[52] P. Pyykko, *Angew. Chem. Int. Ed.* **2004**, *43*, 4412–4456.

[53] V. W. Yam, E. C. Cheng, *Chem. Soc. Rev.* **2008**, *37*, 1806–1813.

[54] M. J. Katz, K. Sakai, D. B. Leznoff, *Chem. Soc. Rev.* **2008**, *37*, 1884–1895.

[55] H. Schmidbaur, A. Schier, *Chem. Soc. Rev.* **2008**, *37*, 1931–1951.

[56] X. He, V. W.-W. Yam, *Coord. Chem. Rev.* **2011**, *255*, 2111–2123.

[57] H. Schmidbaur, A. Schier, *Chem. Soc. Rev.* **2012**, *41*, 370–412.

[58] Mechano-triggered SCSC phase transition at high temperature (near the thermal phase transition temperature) was previously, reported: see reference [2]. Complexes **1** and **2** are the first example of mechano-triggered SCSC phase transition at room temperature. It should be noted that the mechanical-triggered phase transition of **1** and **2** occured at a temperature that is much lower than the thermal transition temperatures.

[59] F. H. Herbstein, *Acta Cryst. B* **2006**, *62*, 341–383.

[60] A. Saeki, S. Seki, Y. Koizumi, T. Sunagawa, K. Ushida, S. Tagawa, *J. Phys. Chem. B* **2005**, *109*, 10015–10019.

[61] A. Saeki, S. Seki, T. Sunagawa, K. Ushida, S. Tagawa, *Philos. Mag.* **2006**, *86*, 1261–1276.

[62] A. Saeki, Y. Koizumi, T. Aida, S. Seki, *Acc. Chem. Res.* **2012**, *45*, 1193–1202.

[63] S. Seki, A. Saeki, T. Sakurai, D. Sakamaki, *Phys. Chem. Chem. Phys.* **2014**, *16*, 11093–11113.

[64] J. D. Dunitz, J. Bernstein, *Acc. Chem. Res.* **1995**, *28*, 193–200.

[65] B. P. Krishnan, K. M. Sureshan, *J. Am. Chem. Soc.* **2015**, *137*, 1692–1696.

[66] M. J. Katz, T. Ramnial, H. Z. Yu, D. B. Leznoff, *J. Am. Chem. Soc.* **2008**, *130*, 10662–10673.

[67] I. M. Sluch, A. J. Miranda, O. Elbjeirami, M. A. Omary, L. M. Slaughter, *Inorg. Chem.* **2012**, *51*, 10728–10746.

[68] The SCSC phase transitions were successful only when the phase changes of **1b** and **2g** started at a single point on the crystals.

[69] This also revealed that the crystalline growth of **2b**, obtained by slow crystallization from solution, occurs preferentially perpendicular to the long axis of the molecule. See Figure S4 for the detailed crystal structure.

[70] G. Han, P. S. Chow, R. B. H. Tan, *Cryst. Growth Des.* **2011**, *11*, 3941–3946.

[71] R. Thakuria, M. D. Eddleston, E. H. Chow, G. O. Lloyd, B. J. Aldous, J. F. Krzyzaniak, A. D. Bond, W. Jones, *Angew. Chem. Int. Ed.* **2013**, *52*, 10541–10544.

[72] S. Ghosh, A. Mondal, M. Kiran, U. Ramamurty, C. M. Reddy, *Cryst. Growth Des.* **2013**, *13*, 4435–4441.

[73] D. Kumar, N. R. Shastri, *Cryst. Growth Des.* **2014**, *14*, 326–338.

[74] Single crystals of $\mathbf{1y_{scsc}}$ and $\mathbf{2b_{scsc}}$ have a low degree of crystallinity and contain some defects that can cause the quenching of an excited state. This is reflected in the superior Φ_{em} values of the solution phase prepared **1y** and **2b** compared with those obtained from the mechano-triggered SCSC phase transitions ($\mathbf{1y_{scsc}}$ and $\mathbf{2b_{scsc}}$, respectively, Table S1).

[75] We confirmed that this phase transition from **1b** to **1y** is monotropic, and no reverse phase transition to **1b** was observed upon cooling to room temperature.

[76] Although there is tiny endothermic peak between 70 and 80°C in the DSC profile of **1y**, microscopic observation of the crystal displays no emission color change. This implies that clear phase transition of **1y** does not take place at this temperature.

[77] We confirmed that this phase transition from **2g** to **2b** is monotropic, and no reverse phase transition to **2g** was observed upon cooling to room temperature.

[78] N. Harada, Y. Abe, S. Karasawa, N. Koga, *Org. Lett.* **2012**, *14*, 6282–6285.

[79] T. Seki, S. Kurenuma, H. Ito, *Chem. Eur. J.* **2013**, *19*, 16214–16220.

[80] N. Blagden, R. J. Davey, *Cryst. Growth Des.* **2003**, *3*, 873–885.

[81] R. J. Davey, *Chem. Commun.* **2003**, 1463–1467.

[82] G. R. Desiraju, *J. Am. Chem. Soc.* **2013**, *135*, 9952–9967.

[83] A. J. Cruz-Cabeza, J. Bernstein, *Chem. Rev.* **2014**, *114*, 2170–2191.

[84] K. H. Kim, Z. Akase, T. Suzuki, D. Shindo, *Mater. Trans.* **2010**, *51*, 1080–1083.

[85] N. Yasuda, H. Uekusa, Y. Ohashi, *Bull. Chem. Soc. Jpn.* **2004**, *77*, 933–944.

[86] The lower Φ_{em} values and lower physical stabilities of the $\mathbf{2b_{scsc}}$ single crystals obtained by mechanical stimulation compared with the solution phase crystallized single crystals of **2b** also supports lower crystal quality in the $\mathbf{2b_{scsc}}$ crystals.

[87] SCSC phase transitions may generate structural defect in the daughter phase unfavorable for the charge transportation. However, the **1y** domain of $\mathbf{1_{IG}}$, which was created by mechano-induced phase transition, does not show significant charging in the SEM observation (bottom half of Figure 10b). Therefore, it is suggested that the lower crystal quality with defect arising from the mechano-induced phase transition process has a smaller effect on the differences in charging of $\mathbf{1_{IG}}$ between the mother and the daughter phases. As discussed in the text, the most plausible reason of the decreased charging in the **1y** domain of $\mathbf{1_{IG}}$ is the formation of multiple aurophilic interactions.

[88] The additional transient absorption spectroscopy revealed that quite short spatial size (~ 10 nm) of statistical local motion of charge carriers in the present TRMC measurement conditions. This result confirms that the present TRMC experiments indeed evaluated the conductivity of the materials that reflects their molecular packing arrangements. See the Supporting Information for more detail.

[89] R. W. Lancaster, P. G. Karamertzanis, A. T. Hulme, D. A. Tocher, T. C. Lewis, S. L. Price, *Eur. J. Pharm. Sci.* **2007**, *96*, 3419–3431.

[90] N. Blagden, R. Davey, R. Rowe, R. Roberts, *Int. J. Pharm.* **1998**, *172*, 169–177.

[91] J.-O. Henck, J. Bernstein, A. Ellern, R. Boese, *J. Am. Chem. Soc.* **2001**, *123*, 1834–1841.

[92] D. K. Bucar, R. W. Lancaster, J. Bernstein, *Angew. Chem. Int. Ed.* **2015**, *54*, 6972–6993.

[93] S. R. Chemburkar, J. Bauer, K. Deming, H. Spiwek, K. Patel, J. Morris, R. Henry, S. Spanton, W. Dziki, W. Porter, J. Quick, P. Bauer, J. Donaubauer, B. A. Narayanan, M. Soldani, D. Riley, K. McFarland, *Org. Process Res. Dev.* **2000**, *4*, 413–417.

[94] We have not confirmed a "disappearing polymorph" in complex **1**.

WILEY-VCH

Entry for the Table of Contents

FULL PAPER

We describe detailed investigation of two intriguing gold(I) complexes that show mechano-triggered single-crystal-to-single-crystal (SCSC) phase transitions, including face index experiments, thermal analyses and conductivity measurements and afforded various hitherto unknown insights into mechano-responsive molecular crystals.

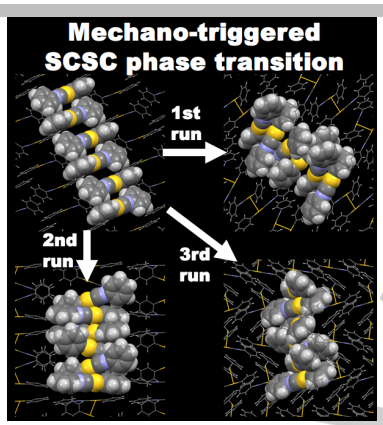

Tomohiro Seki,[a] Kenta Sakurada,[a] Mai Muromoto,[a] Shu Seki[b,c] and Hajime Ito[a]*

Page No. – Page No.

Detailed Investigation of the Structural, Thermal, and Electronic Properties of Gold Isocyanide Complexes with Mechano-Triggered Single Crystal to Single Crystal Phase Transitions

WILEY-VCH